J Solid State Electrochem (2003) 7: 435–441
DOI 10.1007/s10008-002-0339-7

ORIGINAL PAPER

K.S. Abou-El-Sherbini · M.H. Askar

Lithium insertion into manganese dioxide polymorphs in aqueous electrolytes

Received: 7 June 2002 / Accepted: 21 October 2002 / Published online: 5 February 2003

Abstract The electrochemical behaviour of the spinel-like $LiMn_2O_4$ was studied in non-aqueous and aqueous saturated alkali nitrate electrolytes in comparison with the layered manganese dioxide δ-MnO_2. The results obtained by galvanostatic and cyclic voltammetry techniques showed that the insertion of Li^+/e^- or H^+/e^- depends on both the host lattice and the type of electrolyte. The spinel-like $LiMn_2O_4$ preferably allowed the insertion of Li^+/e^- in non-aqueous and aqueous saturated $LiNO_3$ electrolytes, as observed from the similarity of the electrochemical behaviour in these electrolytes and the stability of the structure. This was explained by the presence of a three-dimensional network of vacant tetrahedral and half-filled octahedral sites in $LiMn_2O_4$, which guarantee high mobility of Li^+ ions. The layered manganese dioxide could be inserted by Li^+/e^- only in non-aqueous electrolytes.

Keywords Spinel-like · $LiMn_2O_4$ · δ-MnO_2 · $LiNO_3$ electrolytes · Lithium insertion

Introduction

Recently, lithium-ion batteries have attracted considerable attention. The advantages of this type of battery are high specific capacity, high specific energy and good lifecycle performance. The spinel-like cathodic material $LiMn_2O_4$, in which the Mn_2O_4 framework provides a three-dimensional (3D) interstitial space for Li^+ ion transport, maintains its structure over the compositional range $Li_xMn_2O_4$ ($0 \le x \le 1$) by changing the average Mn oxidation state between 3.5 and 4.0 [1, 2, 3].

Commercial lithium batteries use organic electrolytes in spite of their high cost and safety precautions. Aqueous lithium-ion cells are not considered because cathode and anode materials that are stable in aqueous solution are not readily available. Dahn and co-workers [4, 5, 6] have proposed the concept of rocking-chair cells in aqueous solution. The cathode and the anode are both complex metal oxides of lithium, e.g. $LiMn_2O_4$ is used as the anode and VO_2 or $Li_{0.36}MnO_2$ is used for the cathode.

In aqueous electrolytes it is important to remember that different host lattices for lithium could be successfully employed as the cathode. Also, different aqueous electrolytes have been used for cycling insertion. Recently, Dahn and co-workers [4, 5, 6, 7] used neutral and alkaline solutions saturated with $LiNO_3$ as the electrolyte, $LiMn_2O_4$ as the anode and VO_2 or $Li_{0.36}MnO_2$ was used as the cathode. Deutscher et al. [8] used 0.1 M LiOH saturated with LiCl as the electrolyte, lithium amalgam or Li/Al alloy as the anode and EMD was used as the cathode. Kanoh et al. [9, 10] used 0.1 M LiCl at pH 7.5 as the electrolyte and $LiMn_2O_4$ was used as the cathode.

Although Li and Dahn [11] confirmed the insertion of Li ions into a manganese dioxide lattice in aqueous electrolytes via pH measurements, the role of the concentration of the Li salt was not explored. Moreover, Weiss et al. [12] have rejected the possibility of Li insertion in saturated $LiNO_3$ aqueous electrolytes into another host lattice ($YBa_2Cu_3O_7$). Also, the possibility of H^+/e^- insertion instead of Li^+/e^- should be considered in MnO_2 lattices. For example, in ramsdellite, the oxygen atoms present at the apex of a trigonal pyramid of cations (indicating sp^3 hybridization) can be easily hydroxylated during reduction in aqueous electrolytes, forming groutite [13]. In this work, the aim is to study the possibility of Li^+ insertion into different MnO_2 modifications in different aqueous electrolytes and whether it is a proton or lithium insertion reaction.

The work described herein was carried out at the Institut für Anorganische und Analytische Chemie, Technische Universität Berlin, Germany

K.S. Abou-El-Sherbini (✉) · M.H. Askar
Inorganic Chemistry Department,
National Research Centre, 31 Tahrir Street,
Dokki, Giza, Egypt
E-mail: kh_sherbini@yahoo.com
Fax: +20-2-3370931

Experimental

All chemicals used were of analytical grade from Merck or Fluka unless otherwise stated.

For the preparation of the spinel-like phase $LiMn_2O_4$, $LiOH \cdot H_2O$ and β-MnO_2 were mixed in a 1:2 ratio in a ball-mortar for 2 h, pressed into pellets under 10 t cm^{-2}, heated at 470 °C for 24 h in air and at 700 °C for 12 h under N_2 [14, 15].

For the preparation of the hydrated, layered δ-MnO_2, $Mn(OH)_2$ was precipitated at 0–5 °C by adding 50 mL of 5.2 M NaOH to 40 mL of 2 M $Mn(NO_3)_2$ and oxidized by bubbling O_2 (200 mL min^{-1}) over night through a glass frit (G1) in a 1 m-long tube (3 cm diameter). The product was washed with water until pH 7 and dried in air at room temperature [16, 17].

The composition of $LiMn_2O_4$ and δ-MnO_2 was determined by elemental analysis using atomic absorption spectrometry for Mn, and flame emission spectrometry for Na. For oxidation state evaluation, both the standard iodometry and oxalate methods were used. The water content of δ-MnO_2 was evaluated from the loss of weight after heating at 200 °C for 2 h. For structural investigations, a powder X-ray diffractometer (Siemens D5000, linear counter) was used with CuKα radiation. For the lattice parameters refinement, a commercial regression program was used. As standard, quartz was used for calibration. The X-ray diffractograms of the prepared samples are shown in Fig. 1 and the chemical analysis results and lattice parameters are presented in Table 1.

Electrochemical reactions were performed in three-electrode cells with a commercial potentiostat. In galvanostatic processes, a current density of 3 mA g^{-1} was used unless otherwise stated. Cyclic voltammetry was performed using a Wenking potentiostat scanner with a scanning rate 76 mV h^{-1}, unless otherwise stated. A Hg/HgO reference electrode was used as the standard electrode in aqueous electrolytes made alkaline with 0.1 LiOH, and a saturated calomel electrode was used in the case of neutral aqueous electrolytes. Li metal was used as both counter and reference electrodes in non-aqueous electrolytes. N_2 was used to sweep O_2 during the electrochemical process in aqueous electrolytes. The working electrodes were pressed as tablets under 3 t cm^{-2} into platinum grid-pressed powder electrodes, with 50% (w/w) graphite (KS6 from Lonza) in respect of manganese dioxide samples and ca. 1% (w/w) PTFE. In some cases, graphite was replaced by 10% (w/w) acetylene black (Strem) to avoid reflections in the X-ray diffractograms.

In the case of lithium insertion studies in aqueous electrolytes, saturated $LiNO_3$ with and without 0.1 M LiOH, saturated $NaNO_3$ and KNO_3 were used as the aqueous electrolytes. N_2 was used to sweep O_2 during the electrochemical process in aqueous electrolytes. 1 M lithium trifluoromethanesulfonate ($LiCF_3SO_3$, Fluka) (dried by heating at 80 °C under strong vacuum for 12 h) dissolved in propylene carbonate (Merck) (dried by 3 Å molecular sieves from Metrohm) and kept with an extra amount of the molecular sieve under a dry oxygen-free argon atmosphere in a glove box (under these drying conditions, the electrolyte contain < 30 µg mL^{-1} water) was used in the non-aqueous electrochemistry.

Results and discussion

The graphite used was tested and proved to be electrochemically inert in the potential window from 2 to 4.5 V vs. Li/Li^+ using 1 M $LiCF_3SO_3$ in propylene carbonate.

In the charge-discharge cycles of the layered manganate, the discharge process was performed first to obtain maximum capacity, as observed from the present results and as recommended by Leroux et al. [18] and Chen and Whittingham [19], who reported a loss in capacity upon starting with the charging.

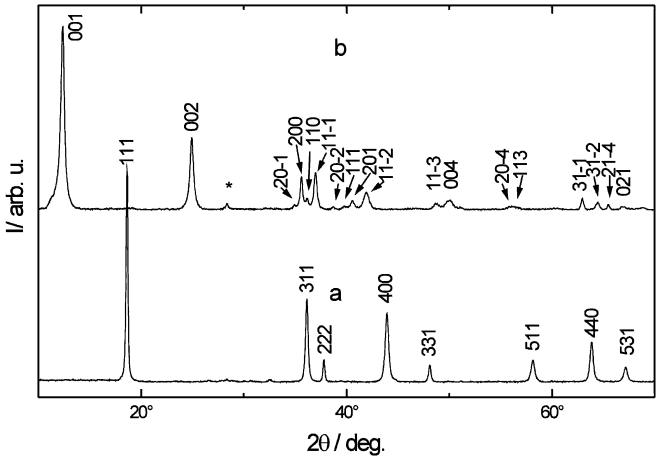

Fig. 1 X-ray powder diffractograms of (*a*) spinel-like $LiMn_2O_4$ and (*b*) δ-MnO_2. The *asterisk* marks the Si sample carrier

Electrochemical behaviour of the spinel-like $LiMn_2O_4$ in a lithium non-aqueous cell

The galvanostatic reduction of the spinel-like $LiMn_2O_4$ after preliminary galvanostatic oxidation to a manganese oxidation state of +3.93, λ-MnO_2 (Fig. 2a), showed the presence of three reduction steps. The first reduction step was observed at a potential of 4.1 V vs. Li/Li^+. The second step occurred from a manganese oxidation state of +3.78 to +3.59 in the potential range 4.03–3.85 V. The reduction was continued to a third step, started at a lower potential (2.85 V). It was accompanied by the reduction of Mn to oxidation state +3.32. To ensure complete utilization of this step, the sample was further discharged at a constant potential of 2 V until the current dropped to < 0.5 mA g^{-1}. The overall charge transfer (240 mA h g^{-1}) and the working potential are in good agreement with previous work [20, 21, 22].

Table 1 Chemical analysis and powder XRD data

Sample	Molecular formula	Oxidation state of Mn	Crystal system	Cell parameters	Error in cell parameters
Spinel-like $LiMn_2O_4$	$LiMn_2O_4$	3.5	Cubic	$a = 8.239$ Å	0.0006
δ-MnO_2	$H_{0.05}Na_{0.34}(H_2O)_{0.5}MnO_2$	3.61	Monoclinic	$a = 5.174$ Å $b = 2.847$ Å $c = 7.330$ Å $\beta = 103.238°$	0.0014 0.0007 0.0021 0.017

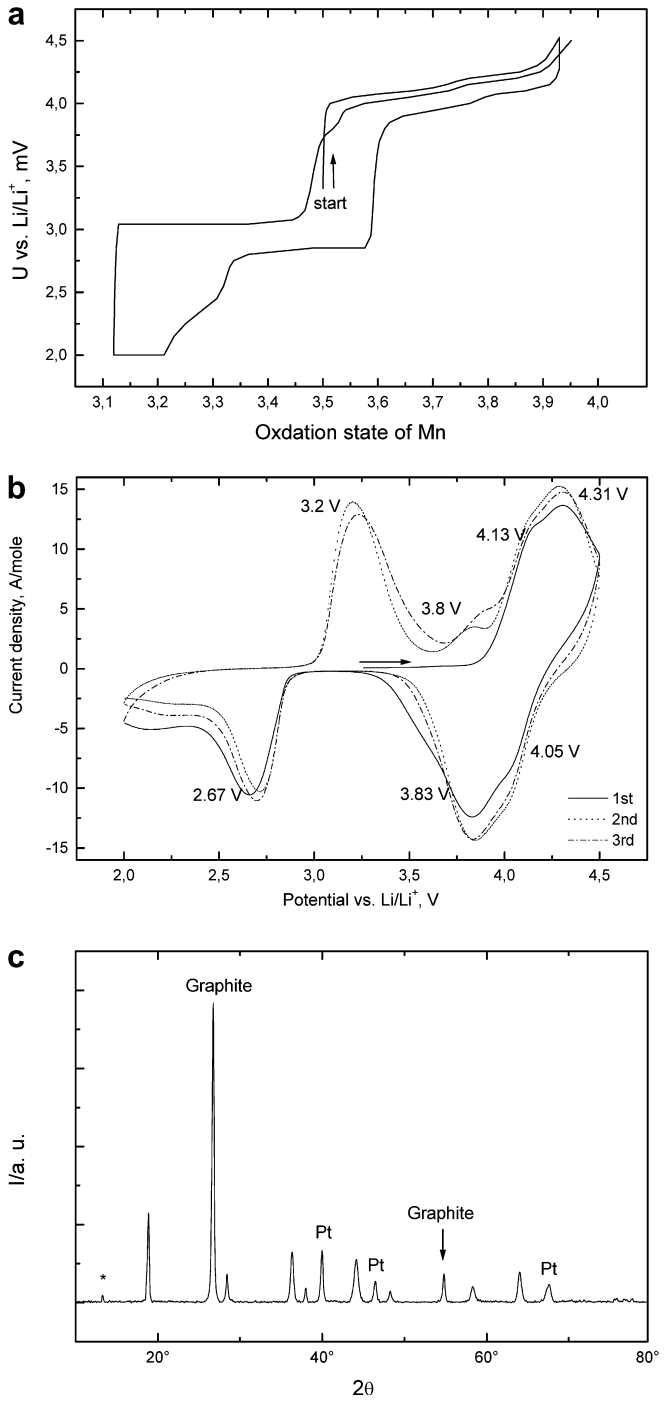

Fig. 2 Oxidation-reduction of spinel-like $LiMn_2O_4$ in 1 M $LiCF_3SO_3$: **a** galvanostatic; **b** cyclic voltammetry with scan rate 288 mV h^{-1}; **c** the X-ray diffraction pattern after the third cycle (the *asterisk* marks an impurity)

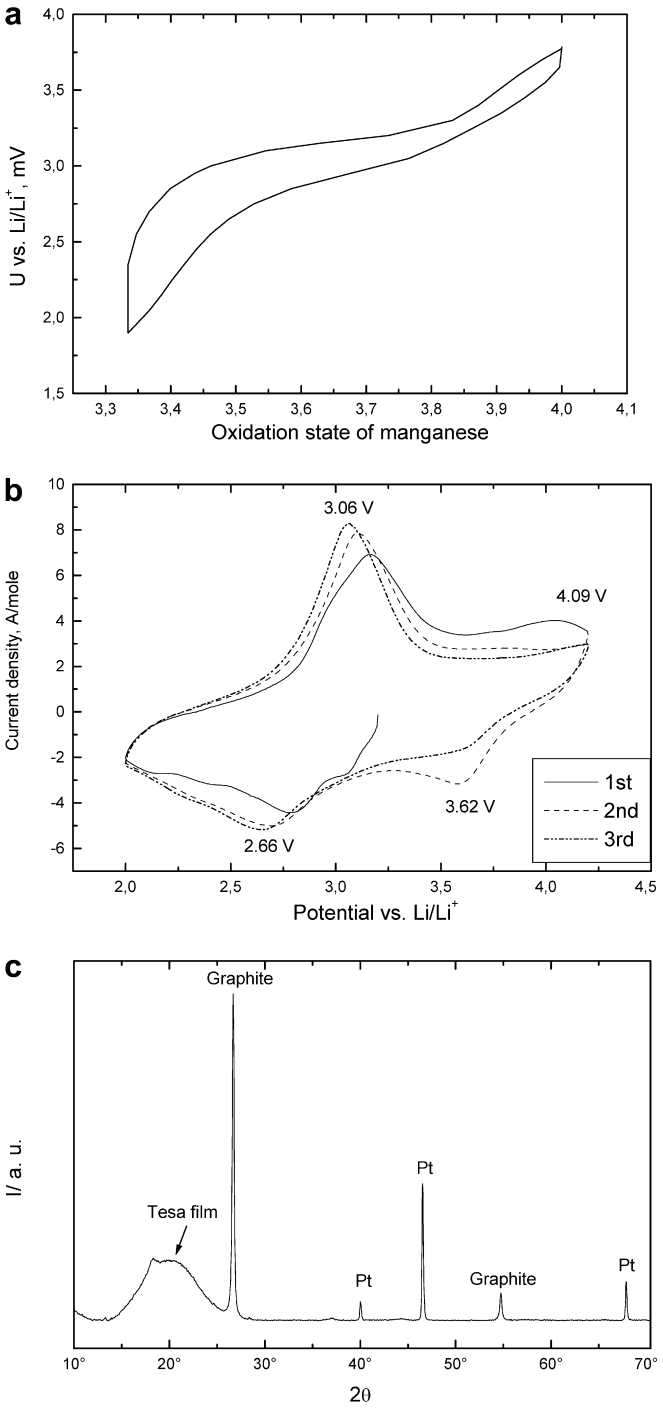

Fig. 3 Reduction-oxidation of δ-MnO_2 in 1 M $LiCF_3SO_3$ under purified argon on a Pt grid: **a** galvanostatic; **b** cyclic voltammetry with a scan rate 288 mV h^{-1}; **c** the X-ray diffraction pattern after the second reoxidation cycle under tesa film

In the recharge process it can be observed that the 3 V process takes place at a potential of 3.31 V, indicating a hysteresis that amounts to 0.5 V, which is very large in comparison with that of the 4 V range which does not exceed 0.08 V, showing the relatively better reversibility of the high-voltage step. The different accommodation sites for lithium ions in the 4 V and 3 V ranges was suggested to be the reason behind this drastic difference in the potential [20, 21, 23].

Cyclic voltammetry (Fig. 2b) showed the presence of three cathodic polarization peaks at 4.05, 3.83 and 2.67 V, three main anodic polarization peaks at 4.31, 4.13 and 3.2 V and a small anodic peak at 3.8 V vs. Li. The reason for the appearance of the last peak is not

known, although it was observed earlier [1]. The positions of the electrochemical steps agree well with previous work [1, 22, 23, 24]. Cyclic voltammetry as well as the X-ray diffraction pattern of the product after three cycles (Fig. 2c) confirmed the excellent reversibility, as a good quality diffractogram was obtained showing the stability of the spinel structure upon insertion and de-insertion of Li ions.

Electrochemical behaviour of the hydrated, layered manganate in non-aqueous electrolytes

The galvanostatic reduction of δ-MnO_2 (Fig. 3a) showed a capacity of 0.67 electron transfer per formula unit (e^-/f.u. or n) or 170 mA h g^{-1}, which is in agreement with that obtained by Strobel and Mouget [17]. The inserted Li^+ ions are believed to be accommodated in the interlayer spacing of the layered δ-MnO_2 and the obtained electron transfer is comparable to the actual vacant sites after subtracting the sites already occupied by Na^+. It is noteworthy to mention that Li^+ present the electrolyte partly exchange with the interlayer Na^+ ions [16].

The rechargeability was observed to be good, as confirmed from the cyclic voltammetry curves (Fig. 3b). These show a cathodic polarization peak at 3.62 V vs. Li/Li^+, which disappeared in the next cycles, and the main reduction peak is at 2.66 V. In the recharge process, the main oxidation peak was observed at 3.06 V and another small shoulder at 4.09 V, which disappeared at the second recharging process.

The X-ray diffraction pattern of the layered MnO_2 after oxidation in the third cycle (Fig. 3c) showed an amorphous phase, which is in agreement with the literature [17].

Electrochemical behaviour of the spinel-like $LiMn_2O_4$ in aqueous electrolyte

The galvanostatic oxidation (charging to λ-MnO_2) of the spinel-like phase $LiMn_2O_4$ in saturated $LiNO_3$ (ca. 4 M) electrolyte can be only reached in the neutral or very weak alkaline solutions because the oxygen evolution potential developed at 640 mV vs. Hg/HgO in saturated $LiNO_3 + 0.1$ M LiOH, before the oxidation of $LiMn_2O_4$ started. The three redox steps observed in the non-aqueous electrolyte could be observed in the galvano-

Fig. 4 The oxidation-reduction reaction of the spinel-like $LiMn_2O_4$ mixed with 9% acetylene black and 1% PTFE: **a** galvanostatic oxidation reduction in saturated $LiNO_3$; **b** cyclic voltammetry in saturated $LiNO_3$; **c** cyclic voltammetry in 1 M $LiNO_3$; **d** X-ray diffraction pattern of the product after the second reoxidation step of **a**. The asterisks mark the stainless steel sample holder

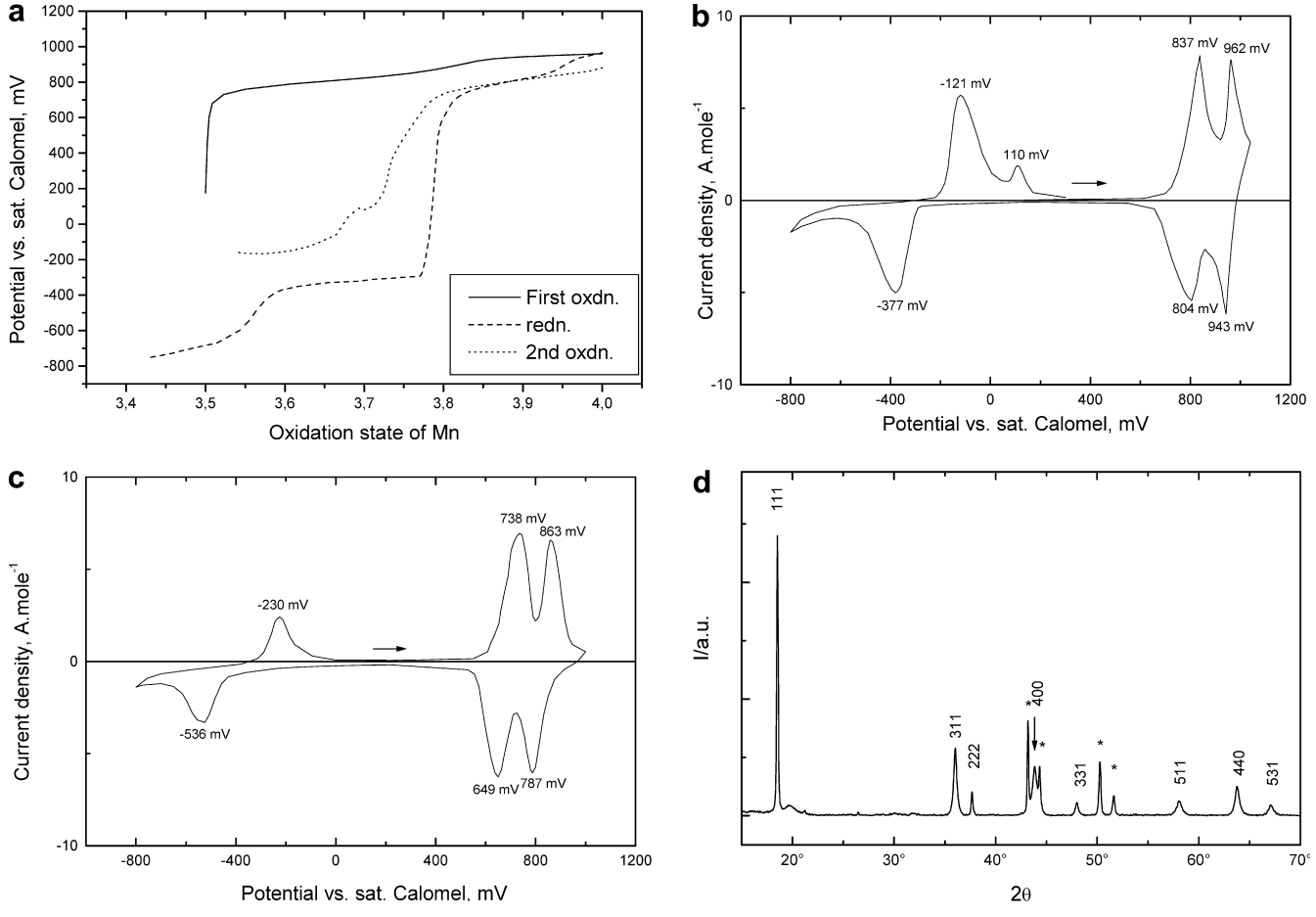

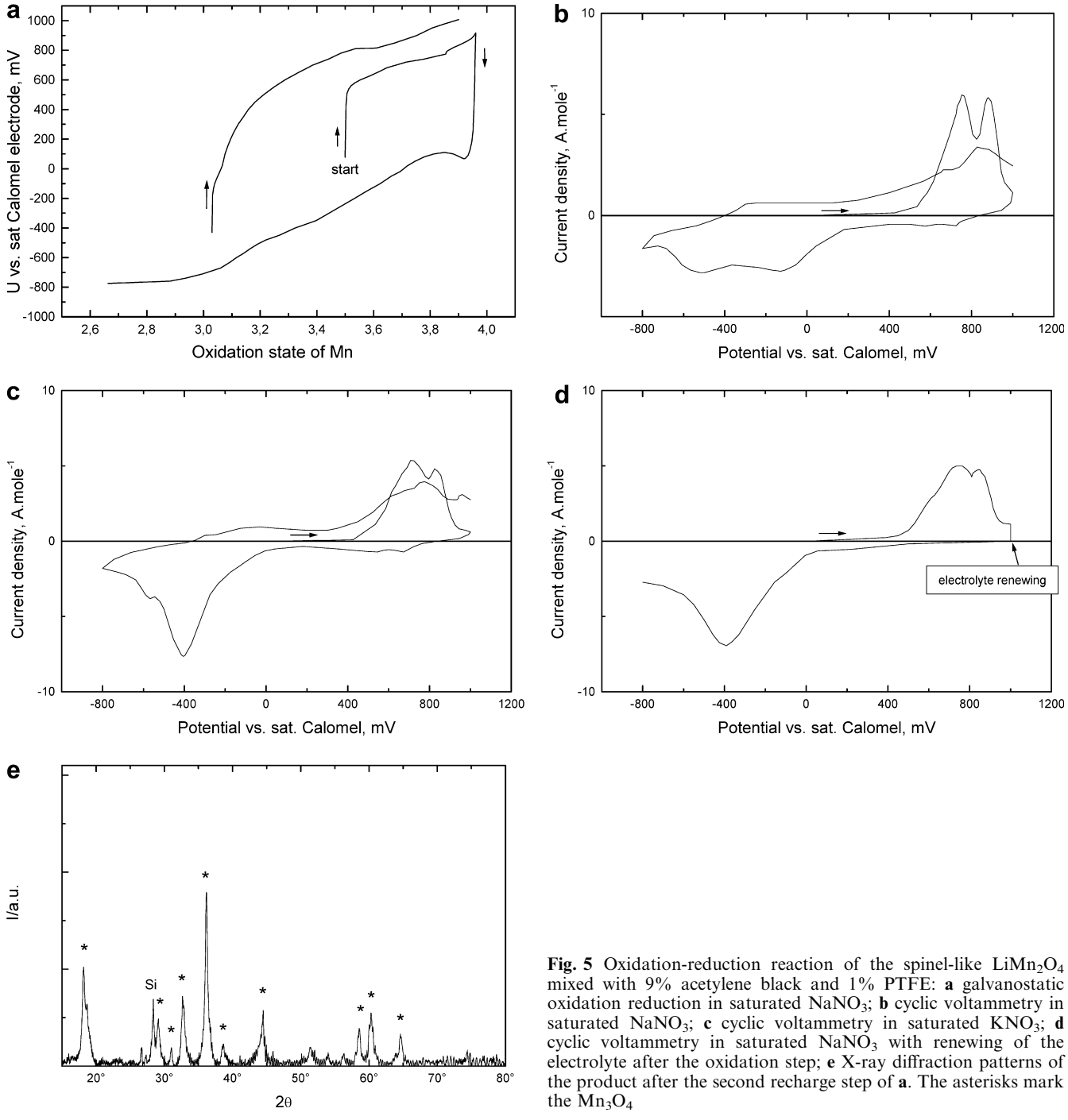

Fig. 5 Oxidation-reduction reaction of the spinel-like $LiMn_2O_4$ mixed with 9% acetylene black and 1% PTFE: **a** galvanostatic oxidation reduction in saturated $NaNO_3$; **b** cyclic voltammetry in saturated $NaNO_3$; **c** cyclic voltammetry in saturated KNO_3; **d** cyclic voltammetry in saturated $NaNO_3$ with renewing of the electrolyte after the oxidation step; **e** X-ray diffraction patterns of the product after the second recharge step of **a**. The asterisks mark the Mn_3O_4

static reduction-oxidation in the neutral, saturated $LiNO_3$ electrolyte with much shorter plateaux, as shown in Fig. 4a. The X-ray diffraction pattern of the product after oxidation of the second cycle (Fig. 4d) showed good stability of the crystal structure.

Cyclic voltammetry of $LiMn_2O_4$ in neutral, saturated $LiNO_3$ electrolyte (Fig. 4b) showed the presence of three cathodic polarization peaks at 943, 804 and –377 mV vs. the saturated calomel electrode (SCE), three main anodic polarization peaks at –121, 837 and 962 mV and a small anodic peak at 110 mV vs. SCE. The present peaks were observed also in the non-aqueous electrolyte, indicating the presence of the same oxidation-reduction mechanism.

The low-potential step which represents the redox reaction $LiMn_2O_4/Li_2Mn_2O_4$ was found to be dependant largely on the concentration of the lithium salt, as in 1 M $LiNO_3$ it was clearly depressed (see Fig. 4c), while the high-potential steps did not change. Also it is important to mention that all the peaks are shifted to more negative values by about 100 mV vs. SCE.

Electrochemical behaviour of the spinel-like $LiMn_2O_4$ in saturated aqueous alkali nitrates

To confirm the lithium insertion mechanism in the aqueous saturated $LiNO_3$ electrolyte, it was important to repeat the same process in other alkali nitrates. Galvanostatic oxidation of $LiMn_2O_4$ in saturated $NaNO_3$ solution (Fig. 5a) took place similar to that in saturated $LiNO_3$ solution. A sudden drop in the potential was observed in the reduction process down to ca. +50 mV vs. SCE, followed by a continuous decrease in the potential which is different from that in saturated $LiNO_3$; the reoxidation pathway also changed.

This was confirmed by cyclic voltammetry of $LiMn_2O_4$ in saturated $NaNO_3$ and KNO_3 solutions (Fig. 5b, c). Only the first oxidation step was similar, whereas there is a small contribution from the high-potential reduction step which may be due to the extracted lithium. This contribution was not observed upon renewing the electrolyte after the first oxidation step (Fig. 5d).

The X-ray diffraction pattern of the product after the second oxidation step (Fig. 5e) showed the destruction of the spinel phase to Mn_3O_4, which was observed during the proton insertion [25].

Accordingly, the electrochemical behaviour of $LiMn_2O_4$ obtained in saturated $LiNO_3$ is due to the saturation of the electrolyte with Li ions and not to the saturation effect as in case of saturated alkali nitrates, where a reduction-oxidation behaviour similar to that obtained in proton insertion mechanism was obtained [25]. Moreover, in aqueous Li salt electrolytes the lithium insertion mechanism into λ-MnO_2 may be adopted.

Electrochemical behaviour of the hydrated, layered manganate in saturated aqueous lithium nitrate

The galvanostatic reduction of the hydrated, layered manganate in saturated $LiNO_3$ (Fig. 6a) with the reduction in alkaline electrolytes showed a similar pathway to that reported previously [26]. A one-phase reaction was found to take place up to electron transfer $0.2n$, followed by a two-phase reaction which ended at electron transfer $0.84n$ accompanied by destruction of the electrode material and the formation of Mn_3O_4, as indicated from the X-ray diffraction pattern of the

Fig. 6 Reduction-oxidation reaction of δ-MnO_2: **a** galvanostatic in saturated $LiNO_3$; **b** galvanostatic reduction oxidation in 0.1 M LiOH, saturated with $LiNO_3$; **c** cyclic voltammetry in 0.1 M LiOH saturated with $LiNO_3$; **d** X-ray diffraction patterns of the product **a** after the reduction process of **a** (bottom) and after the third oxidation step of **c** (top). The asterisks mark $LiNO_3$; + Mn_3O_4; Si = silicon sample holder and Gr = graphite

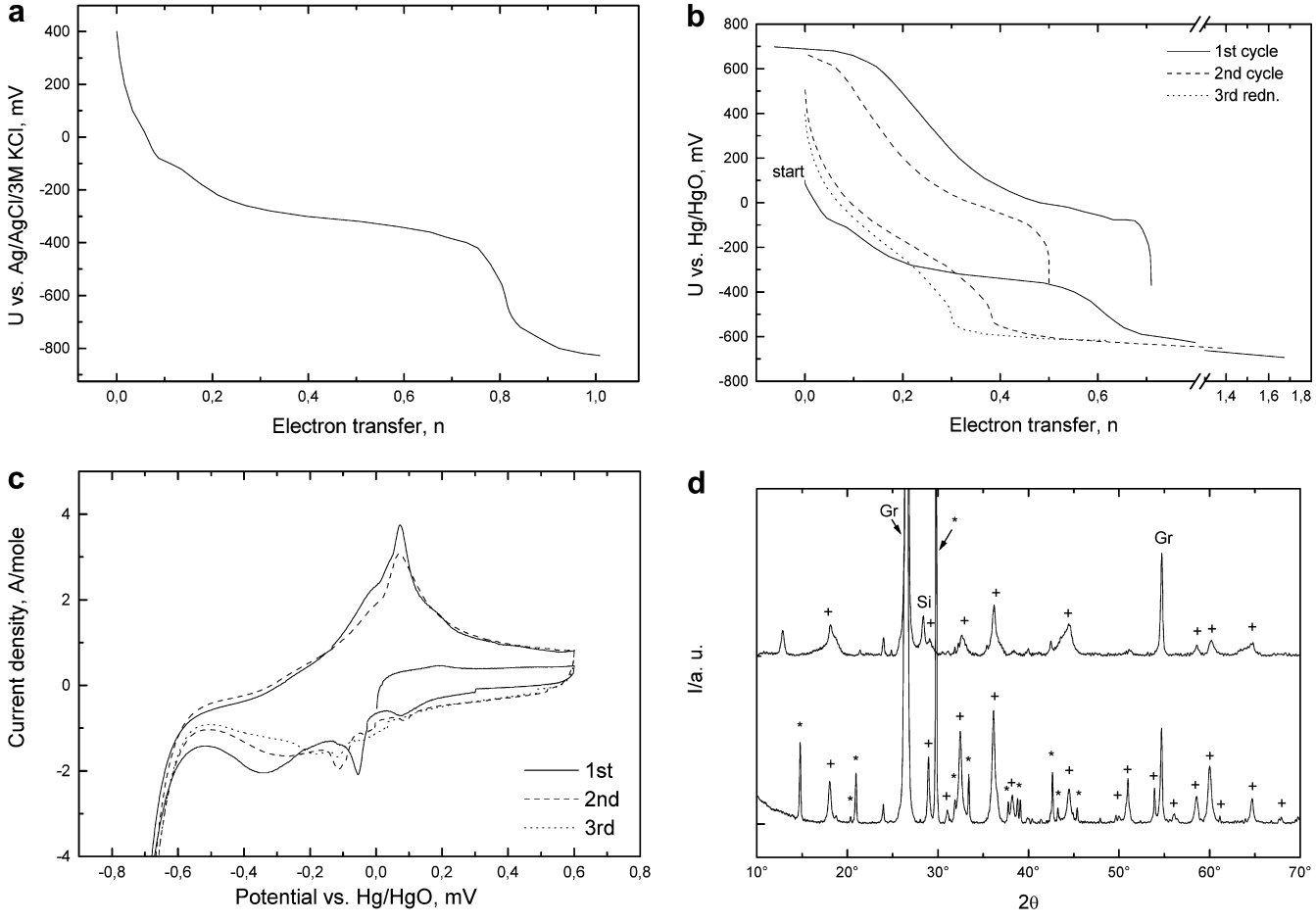

product (Fig. 6d, bottom). The destruction of the electrode material is due to dissolution of the hydrated, layered manganate during reduction due to the low pH of the electrolyte (pH 5–6).

The rechargeability of hydrated, layered manganate could be studied using 0.1 M LiOH saturated with $LiNO_3$ (Fig. 6c), as the alkaline electrolyte prevented the dissolution of the electrode material. The galvanostatic reduction-oxidation curves showed a capacity fading in the first three cycles. This was due to the accumulation of the Mn_3O_4, as observed from the X-ray diffraction pattern of the product after the third oxidation cycle (Fig. 6d, top).

Cyclic voltammetry of the hydrated, layered manganate in 0.1 M LiOH saturated with $LiNO_3$ (Fig. 6c) confirmed the results obtained from the galvanostatic curves. The anodic and cathodic polarization peaks of the reversible one-phase reaction observed at +195 and +76 mV vs. Hg/HgO, respectively, were shifted by about 50 mV to more positive values. Two cathodic polarization peaks were observed at –54 and –340 mV and two anodic polarization peaks in the recharge step at –17 and 76 mV. The cathodic polarization peak at –54 mV was shifted to a more negative value in the next cycle.

Conclusion

The redox process of the spinel-like phase $LiMn_2O_4$ in saturated aqueous $LiNO_3$ solution is reversible in spite of the great capacity loss, which may be due to the dissolution of the electrode material in the electrolyte. Also, the low-potential step depends strongly on the concentration of the lithium salt. The mechanism of the redox reaction of $LiMn_2O_4$ in saturated $LiNO_3$ solution is very likely to be a lithium insertion reaction as in the non-aqueous cells, which was suggested by Dahn and co-workers [4, 5, 6, 7, 11].

Furthermore, the attempt to insert lithium into the hydrated, layered manganate using saturated lithium nitrate electrolytes, in a similar way to the spinel phase (this work and others [4, 5, 6, 7]) and the γ-MnO_2 [8], did not succeed. This may be understood in view of the site availability and the rate of diffusion, as both the spinel-like $LiMn_2O_4$ and γ-MnO_2 phases are attractive host structures for lithium insertion/extraction reactions because they provide a 3D network of face-sharing tetrahedra and octahedra for lithium ion diffusion. In contrast, the hydrated, layered manganate provides only tetrahedral sites sharing three faces with MnO_6 octahedra, which are the most unfavourable sites for lithium accommodation owing to the metal-metal repulsion [2, 27].

Acknowledgements The authors wish to express their deep gratitude to Prof. R. Schöllhorn and his research group, Institut für Anorganische und Analytische Chemie, Technische Universität Berlin, Germany, for valuable cooperation and discussion.

References

1. Thackeray MM (1997) Prog Solid State Chem 25:1
2. Thackeray MM (1995) J Electrochem Soc 142:2558
3. Thackeray MM (1992) Prog Batt Batt Mater 11:150
4. Li W, Dahn J, Wainwright D (1994) Science 264:1115
5. Li W, McKinnon R, Dahn J (1994) J Electrochem Soc 141:2319
6. Li W, Dahn J (1995) J Electrochem Soc 142:1742
7. Zhang M, Dahn J (1996) J Electrochem Soc 143:2730
8. Deutscher R, Florence T, Woods R (1995) J Power Sources 55:41
9. Kanoh H, Feng Q, Hirotsu T, Ooi K (1996) J Electrochem Soc 143:2610
10. Kanoh H, Hirotsu T, Ooi K (1996) J Electrochem Soc 143:905
11. Li W, Dahn J (1995) J Electrochem Soc 142:744
12. Weiss M, Günther W, Schöllhorn R (1998) Physica C 304:156
13. Chabre Y, Pannetier J (1995) Prog Solid State Chem 23:107
14. Xia Y, Noguchi H, Yoshio M (1995) J Solid State Chem 119:216
15. Xia Y, Takeshige H, Noguchi H, Yoshio M (1995) J Power Sources 56:61
16. Le Goff P, Baffier N, Bach S, Pereira-Ramos J-P (1996) Mater Res Bull 31:63
17. Strobel P, Mouget C (1993) Mater Res Bull 28:93
18. Leroux F, Guyomard D, Piffard Y (1995) Solid State Ionics 80:299
19. Chen R, Whittingham M (1997) J Electrochem Soc 144:L64
20. Miura K, Yamada A, Tanaka M (1996) Electrochim Acta 41:249
21. Ohzuku T, Kitagawa M, Hirai T (1990) J Electrochem Soc 137:769
22. Koksbang R, Barker J, Saïdi M, West K, Zachau-Christiansen B, Skaarup S (1996) Solid State Ionics 83:151
23. Xia Y, Yoshio M (1997) J Power Sources 66:129
24. Saïdi M, Barker J, Koksbang R (1996) Electrochim Acta 41:199
25. Schlörb H, Bungs M, Plieth W (1997) Electrohim Acta 42:2619
26. Abou-El-Sherbini Kh, Askar M, Schöllhorn R (2002) Solid State Ionics 150:417
27. Voinov M (1982) Electrochim Acta 27:833